We are IntechOpen,
the world's leading publisher of
Open Access books
Built by scientists, for scientists

6,900
Open access books available

185,000
International authors and editors

200M
Downloads

154
Countries delivered to

Our authors are among the

TOP 1%
most cited scientists

12.2%
Contributors from top 500 universities

CLARIVATE ANALYTICS
BOOK CITATION INDEX
INDEXED

WEB OF SCIENCE™

Selection of our books indexed in the Book Citation Index
in Web of Science™ Core Collection (BKCI)

Interested in publishing with us?
Contact book.department@intechopen.com

Numbers displayed above are based on latest data collected.
For more information visit www.intechopen.com

Dynamic Speckle Interferometry of Technical and Biological Objects

Alexander Vladimirov

Abstract

The theory of speckle dynamics in the image plane of a reflecting and thin transparent object is considered. It was assumed that the optical paths of the reflected and probing transparent object waves vary due to (1) translational motion, (2) oscillations with a period T, and (3) random relative displacements of pairs of scattering centers Δu (reflecting object) and random changes in the refractive index Δn (transparent object). The formulas relating the mean value, dispersion, and relaxation time of Δu and Δn values with the time-averaged radiation intensity at the observation point and the time autocorrelation function of this intensity are obtained. It is shown that at the averaging time multiple of T, the technique in real time allows to determine plastic deformations of the order of 10^{-3} on bases of the order of 10 microns, which is suitable for the control of elastic deformations on bases of the order of 100 microns. The possibilities of the method of averaged speckle images for the study of (1) features of the nucleation, start, and movement of the fatigue crack, and (2) the activity of living cells infected and not infected with the virus are demonstrated.

Keywords: theory, experiment, high cycle fatigue, live cell, speckle dynamics, estimation of time to failure, crack nucleation

1. Introduction

If a rough object is illuminated by coherent radiation, macroscopically homogeneous but microscopically inhomogeneous distribution of scattered radiation intensity emerges at some distance from the object and behind the lens that forms the object image. As the surface microrelief heights are random, the waves reflected from various microscopic areas of the surface have random amplitudes and phases. Mutual interference of these waves results in spotted or "speckle" structure of scattered radiation. When the object surface varies for some reason, the amplitudes and phases of the reflected waves change, so the speckle pattern also varies. Variation of wave amplitudes and phases can be caused by displacement of the object or its rigid rotation or by small variations in the distances between the area elements due to elastic or plastic strains of the surface. The reason may be a small or strong surface microrelief variation due to corrosion or loosening of the material with ionizing radiation, material fatigue, etc. The specified macroscopic or microscopic processes can occur simultaneously.

It is noteworthy that the speckle pattern can be formed when studying objects with a mirror surface by lighting them via mat glass. Phenomena occurring inside

transparent objects can be studied in a similar way. Such objects are live cells cultured or precipitated on a transparent substrate. If there is an empty space, the cells can alter their shape and the intracellular processes randomly change the phases of the waves that have passed via the cell. So, by the character of the speckle pattern change, one can study and monitor the phenomena occurring on the surface or near the surface of reflecting objects or inside transparent media.

At present, one is familiar with application of variations, displacements, and interferences of speckle fields for the study of macroscopic phenomena, namely, for determination of transition, motion velocity, rotations, elastic or plastic strains of objects, gas, and fluid flows [1–7]. At the same time, the logic of speckle optics development and practical needs sets the task to analyze not only macroscopic but also microscopic processes occurring at the structural level. For example, a task like that appears in studies of the phenomena accompanying crack initiation in high-cycle fatigue of metallic materials as well as during the analysis of the processes occurring in the membranes and inside the cells of live systems. The rationale for such studies is related to development of a technique for assessing the remaining life of construction elements, and in case of biological objects, to individualized drug selection for a patient.

As the properties of materials are random at the structural level, the amplitudes and phases of the waves reflected from the object or that have passed through the object randomly vary in time and space. In the general case, the solution to the problem of establishing a relation between the parameters of wave phase dynamics and speckle dynamics is far from simple. Nevertheless, lately certain advances in solving such problems have been observed.

The objective of this publication is to familiarize the readers with the author's recent developments in the theory and application of dynamic speckle interferometry. They were aimed at study of the processes occurring in technical materials in their high-cycle fatigue and also in live cells subject to some external effects. The rationale for the specified studies, for the theory of the techniques proposed, the conducted experiments and their practical prospects are discussed in brief. The advantage of the techniques under discussion over the conventional speckle holographic techniques is the possibility for real-time study of reversible and irreversible processes. Most part of this chapter is devoted to dynamic speckle interferometry of high-cycle fatigue. When high-cycle fatigue is studied, the technique permits determination of the limiting local microrelief and surface shapes variations (deformations) with high sensitivity. When the variation rate of the named values is monitored, the time to the fatigue crack start can be determined. When the reaction of cells to viruses and bacteria is studied, an opportunity for timely development of procedures preventing and blocking their development progress appears.

2. High-cycle fatigue: the problems and the rationale for the studies

When technical objects are exploited, their various elements are affected by alternate forces. As load cycle number N in the materials increases, their properties change irreversibly resulting in fracture of the construction elements. In the literature, this phenomenon was called material fatigue. Depending on number N_a, of the cycles preceding the fracture, we distinguish low-cycle, high-cycle, and giga-cycle fatigue. Their borders are rather blurred. It is usually supposed that a part was destroyed in low-cycle fatigue if $N_a < 10^4$. If a part is exploited at $10^5 < N < 10^7$, then high-cycle fatigue is supposed, and at $N > 10^8$, the part is supposed to be exploited in giga-cycle fatigue.

At present, various features of low-cycle fatigue are fairly well characterized [8, 9]. It is explained by the fact that in low-cycle fatigue, sufficient plastic

deformations of the objects normally appear. That is why conventional approaches developed for devices exploited under the conditions of quasi-static loading are applicable for monitoring and estimating of the remaining object life.

The situation with high-cycle as well as giga-cycle fatigue is different. According to various literature sources, from 50 to 80% of equipment is destroyed due to high-cycle fatigue [10–12]. Despite research history [13–16] and a great number of publications [17, 18], at present, there are no techniques for assessment and estimation of the remaining life of construction elements in their high-cycle fatigue that would meet the requirements of the engineering practice [11, 18]. According to [11, 18, 19], the situation has arisen due to absence of physical models of high-cycle fatigue. In the author's opinion, this circumstance is in turn related to absence of physical monitoring techniques that would permit to record the features of local fatigue damage accumulation without interruption of exploitation or fatigue testing of various objects. Analysis of studies [20–25] devoted to development of such methods shows that their practical application implies methodological issues.

Immediately after the creation of lasers and detection of spotted or speckle structure of scattered radiation, speckles were used to study fatigue phenomena [26–28]. However, because of high manpower effort and no monotone character of the recorded signal variation, the technique was not put to wide use.

The author learnt the difficulties of fatigue phenomena studies using conventional nondestructive testing techniques at first hand. Early in our research aimed at the study of high-cycle material fatigue, we used various modifications of optical, X-ray, magnetic, electric, and acoustic techniques (13 in all). The results obtained using these techniques were negative. The parameters of the signals either did not vary or the variations were at the same level as the hardware noise. As in high-cycle fatigue localization of fatigue damage takes place [11], it was supposed that the obtained negative result is related to a large base (averaging region) of the applied techniques. Hence, for measurements on a small base, we upgraded a speckle technique that was previously successfully used to monitor the damage in quasi-static deformation of specimens up to their fracture [29, 30].

Section 3 presents the results of the theoretical studies aimed at developing an optical technique intended to study the irreversible processes emerging while testing specimens for high-cycle fatigue. Section 4 discusses the experiments with high-cycle fatigue conducted using this technique.

3. Theory

This section discusses the results of theoretical underpinning of speckle techniques permitting the study of fatigue accumulation in periodical deformations of the objects. Sections 3.1 and 3.2 discuss the regularities of speckle dynamics observed while capturing the frames of the speckle image on fixed position of the object oscillations. Section 3.3 is dedicated to the theory of time-averaged speckle images.

3.1 Dynamic speckle interferometry of microscopic processes: reflecting object

Let the source of coherent radiation with wavelength λ located at point $\vec{s}$ illuminate the point scattering centers located in some region S in plane (x, y), as is shown in **Figure 1**.

A thin lens with focal distance f and diaphragm diameter D located in plane (η_x, η_z) forms the object image in plane (q_x, q_y). We regard all the waves at hand as linearly polarized in the same direction. We accept that phase φ_j of complex amplitude a_j of a wave scattered by the j-th center is random, and that the waves from all the scattering
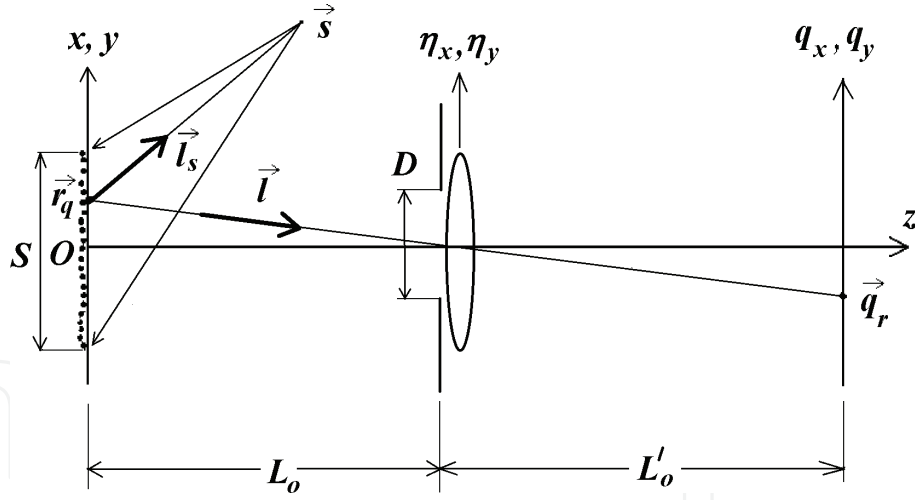
Figure 1.
Optical system for reflecting objects and designations.

centers come to an arbitrary point of plane (η_x, η_y). First, let us obtain an expression for radiation intensity $I(\vec{q})$ at some point $\vec{q}$ of the object image plane. For total complex amplitude $A(\vec{\eta})$ at arbitrary point $\vec{\eta}$ of plane (η_x, η_y), we have:

$$A(\vec{\eta}) = \sum_{j=1}^{N} a_j, \tag{1}$$

where N is the number of scattering centers. We will get the complex amplitude of light $A(\vec{q})$ at point $\vec{q}$ adding up the amplitudes of the waves that came from the points of plane (η_x, η_y) to point $\vec{q}$, considering amplitude $P(\vec{\eta})$ and phase $\exp\left[i|\vec{\eta}|^2/(2f)\right]$ transmission of the lens [3]:

$$A(\vec{q}) = \int\limits_{-\infty}^{+\infty}\!\!\int P(\vec{\eta}) e^{\frac{i|\vec{\eta}|^2}{2f}} e^{ik|\vec{L}_q(\vec{\eta})|} \sum_{j=1}^{N} a_j \, d\eta_x d\eta_y, \tag{2}$$

where i is an imaginary unit and $\vec{L}_q(\vec{\eta})$ is a vector targeted from point $\vec{\eta}$ to point $\vec{q}$.

Let us take the relation between complex amplitude of light in proximity of point $\vec{r_j}$ and at point $\vec{\eta}$ in the same form as in [3]:

$$a_j(\vec{\eta}) = \sqrt{I_0(\vec{r_j})}\, \xi(\vec{r_j})\, e^{i\left\{k\left[|\vec{L}_s(\vec{r_j}+\vec{u}_j)|+|\vec{L}_\eta(\vec{r_j}+\vec{u}_j)|\right]+\phi_j\right\}}, \tag{3}$$

where $I_0 = I_0(\vec{r})$ is the distribution intensity of the illuminating radiation, $\xi = \xi(\vec{r})$ in the general case is the complex reflection coefficient that takes into account the proportion of the radiation going from point $\vec{r}$ to point $\vec{\eta}$, $\vec{L}_s(\vec{r})$ is the vector targeted from point $\vec{r}$ to point $\vec{s}$, $\vec{L}_\eta(\vec{r})$ is the vector targeted from point $\vec{r}$ to point $\vec{\eta}$, $\vec{u}_j$ is the vector of small displacement of the j-th center.

Let us take arbitrary point $\vec{q} = \vec{q}_r$ and its conjugated point $\vec{r}_q$. It is known that a wave going from point $\vec{r}_q$ forms an Airy pattern as the result of light diffraction on a diaphragm with diameter D and the center at point $\vec{q}_r$. The radius of central spot b_s of the pattern equals 1, $22\lambda L_0'/D$, where L_0' is the distance from the lens to plane (q_x, q_y). Region with radius $a_s = b_s/m$, where m is the magnification of the lens, corresponds to regions with radius b_s in plane (x, y). It is known that 85% of the energy of the wave that passed via the lens falls on the central spot of the Airy pattern. We will neglect the energy that falls on the sections beyond the region with radius b_s. This in turn means that we suggest that the waves from the scattering centers located only in the region with radius a_s with the center at point $\vec{r}_q$ come to point $\vec{q}_r$. Now, let N be the number of such centers.

Let us further assume that the region with radius a_s, values D, and $\left| \vec{u} \right|$ is small compared to the distances from the object to the radiation source and to the lens as well as that from the lens to the image plane. Regarding expression $\left| \vec{L}_s \right| = \left| \vec{L}_s \left(\vec{r} + \vec{u} \right) \right|$ as continuous function $\vec{r}$ and $\vec{u}$, let us expand it in a Taylor series in a small neighborhood of point $\vec{r} = \vec{r}_q$, $\vec{u} = 0$, taking into account the derivatives to the first-order inclusive. Let us similarly expand expression $\left| \vec{L}_\eta \left(\vec{r} + \vec{u} \right) \right|$ in the vicinity of points $\vec{r} = \vec{r}_q$, $\vec{\eta} = 0$, and $\vec{u} = 0$, and expression $\left| \vec{L}_\eta \left(\vec{q} \right) \right|$ in the vicinity of points $\vec{\eta} = 0$ and $\vec{q} = \vec{q}_r$. One can familiarize oneself with the results in specified expansions in [31, 32]. Taking the obtained expansion, as well as formulas (3) and (2) into account, we in [31] obtained an expression for $A\left(\vec{q} \right)$ and $I\left(\vec{q} \right)$:

$$A\left(\vec{q} \right) = \sqrt{I_{01}} e^{i\psi_j} \sum_{j=1}^{N} e^{i\left\{ k\left[\vec{u}_j \left(\vec{l}_s + \vec{l} \right) \right] + \theta_j \right\}}, \tag{4}$$

$$I\left(\vec{q} \right) = A\left(\vec{q} \right) \times A^*\left(\vec{q} \right) = I_{01}N + 2I_{01} \sum_{\kappa=1}^{K} \cos\left[\Delta\phi_\kappa + \Delta\theta_\kappa \right], \tag{5}$$

where $\vec{l}_s = \vec{l}_s \left(l_{sx}, l_{sy}, l_{sz} \right)$ and $\vec{l} = \vec{l} \left(l_x, l_y, l_z \right)$ are unit vectors targeted from point $\vec{r}_q$ to the radiation source and to the observer, respectively; $\theta_j = k\vec{r}_j \left(\vec{l}_s + \vec{l} \right) + \varphi_j$, complex amplitude $\sqrt{I_{01}} e^{i\psi_j}$ determines the expression preceding the summation sign; $\Delta\phi_\kappa = k\Delta u_\kappa = k\Delta\vec{u}_\kappa \left(\vec{l}_s + \vec{l} \right)$, $\Delta\vec{u}_\kappa$ is the relative displacement vector of the κ-th pair of scattering centers; and $\Delta\theta_\kappa = \theta_j - \theta_m, j \neq m, \kappa = 1, 2...K, K = N(N-1)/2$.

Then, let us assume that process $\Delta u_\kappa(t)$ is random, and for a fixed κ, there is correlation of values Δu_κ in time. Assuming that all the random values are independent, in [31], we obtained an expression for temporal normalized autocorrelation function of radiation intensity $\eta_{1,2}(t_1, t_2)$ at point $\vec{q}$:

$$\eta_{1,2}(t_1, t_2) = \cos\left[\langle x_2 \rangle - \langle x_1 \rangle \right] \times e^{-\frac{1}{2}k_{11} - \frac{1}{2}k_{22} + k_{12}}, \tag{6}$$

where $\langle x_1 \rangle$ and $\langle x_2 \rangle$ are values $\Delta\phi_\kappa$ average by the ensemble of objects at time points t_1 and t_2, respectively, k_{11} and k_{22} are variances of values $\Delta\phi_\kappa$ at time points t_1 and t_2, respectively, and k_{12} is the correlation coefficient of phase differences $\Delta\phi_\kappa$ at time points t_1 and t_2.

If process $\Delta u_\kappa(t)$ is stationary, then $\langle x_1 \rangle = \langle x_2 \rangle$ and $k_{11} = k_{22}$, and instead of (6), we have:

$$\eta(\tau) = e^{-k_{11}+k_{11}\rho_{12}(\tau)}, \tag{7}$$

where $\rho_{12}(\tau)$ is a normalized autocorrelation function of relative displacements, $\tau = t_2 - t_1$. From (7), it follows that if τ exceeds correlation time τ_0 of values Δu_κ, function $\eta(\tau)$ levels off to $\eta^* = \exp(-k_{11})$. In our experiments discussed below, this circumstance was used to determine value k_{11} as the parameter of fatigue damage to the specimens.

At values Δu_κ that are small compared with λ, it is convenient to exclude the permanent part of $\eta = \eta^*$, proceeding to a new normalized autocorrelation function $\eta'(\tau) = [\eta(\tau) - \eta^*]/[\eta(0) - \eta^*]$. It is easy to show that at $\Delta u_\kappa \ll \lambda$, we have $\eta'(\tau) \cong \rho_{12}(\tau)$. Therefore, the corresponding normalized spectral functions $g_I(\omega)$ of intensity fluctuation and relative displacements $g_{\Delta u}(\omega)$ are equal. The correlation (relaxation) times τ_0 of values Δu_κ and fluctuations of radiation intensity τ_κ in the conjugated region are also equal.

At $\Delta u_\kappa \geq \lambda$, establishing a relation between $g_{\Delta u}(\omega)$ and $g_I(\omega)$ is not a simple task. In [33], it was done for the case when function $\rho_{12}(\tau)$ is a Gaussian function. It was shown that in this case, $g_{\Delta u}(\omega)$ and $g_I(\omega)$ are also Gaussian functions, with the function range $g_I(\omega)$ at level 1/e is k_{11} times as wide as that of function $g_{\Delta u}(\omega)$.

3.2 Theory of speckle dynamics of microscopic processes: transparent object

Let us discuss an optical system (**Figure 2**) that forms an image of a thin transparent (phase) object. Let the source of coherent light 1 illuminate thin diffuser 2 consisting of point stationary diffusers chaotically located near plane (x,y). The waves spreading from point centers first pass through various sections of thin transparent object 3 and then via lens with diagram 4. Planes (x,y) and (q_x,q_y) are conjugated. Let us accept that the sum of the diffuser thickness, the distance from the diffuser to the object, and the object thickness are less than the longitudinal resolution of the lens. To simplify the calculations, let us suggest that the refraction indexes of the medium inside and outside the diffuser are same and equal 1. Let us assume that the optical paths of the sounding waves in the object 3 randomly change, in time, and let us neglect the refraction of waves within the object. Let us take the conjugated points 6 and 7. Reasoning the same way as we did in Section 3.1,
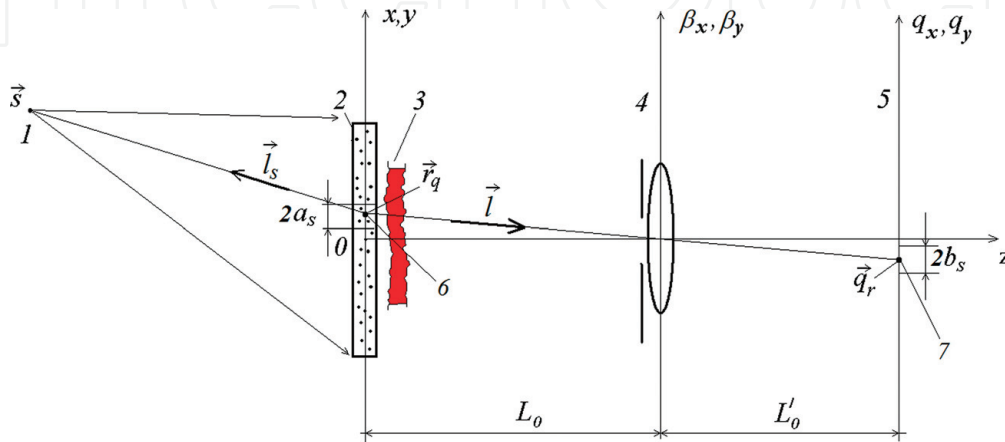

Figure 2.
Optical system for a transparent object: 1—light source, 2—diffuser, 3—transparent object, 4—lens with diaphragm, 5—image plane, and 6 and 7—conjugated points.

we can obtain an expression for radiation intensity $I\left(\vec{q}\right)$ at point 7, and also for normalized autocorrelation function $\eta(t_1, t_2)$ of this intensity. Such calculations were performed in [33]. It was obtained that the expression for $\eta(t_1, t_2)$ is precisely formula (6), but the value Δu_κ is determined by a different formula:

$$\Delta u_\kappa = u_j - u_m \tag{8}$$

where κ is the wave pair number again, and

$$u_j = \int\limits_{l_j} [n(l) - n_0] dl, \, u_m = \int\limits_{l_m} [n(l) - n_0] dl, \tag{9}$$

are the optical path lengths of the j-th and m-th sounding waves, respectively; l_j and l_m are the paths of the corresponding waves, and $n(l)$ is the distribution of the refraction index along the wave path. The above features of functions $\eta(t_1, t_2)$ and $g_{\Delta u}(\omega)$ remain valid.

3.3 Theory of time averaging method for speckle images

The results of the theory discussed above in Sections 3.1 and 3.2 were used in studies of irreversible processes arising in metals with their high-cycle fatigue [31, 34] and in live cells [35]. In the cases when spatially homogeneous and temporally stationary random variation of optical wave paths occurred at the structural level, good coincidence between the theory and the experiment was observed.

However, the drawback of the theories discussed in Sections 3.1 and 3.2 is the difficulty of application in the cases when random variations of the wave phases occur due to various simultaneous processes occurring at different rates.

For example, in high-cycle metal fatigue, the phase of the wave reflected from part of the surface can vary as a result of translational motion of the object, its elastic or plastic deformation, phase transformation, and formation of microcracks.

When a live cell is studied, the wave phase can vary due to diffusion of the substances through the membrane, endocytosis (capture of large particles due to local cell shape variation), and protein synthesis as well as cell motion.

To overcome the drawback named in [32, 36, 37], the theory was upgraded. The idea consisted in application of the time averaging procedure to speckle dynamics. If the characteristic time τ_0 of wave phase variation corresponding to the fastest process is known, then the averaging time T_1 of the recorded optical signals can be taken larger than τ_0. In this case, speckle dynamics will be formed due to occurrence of slower processes; moreover, interpretation of the experimental data can get simplified.

Let us discuss the results of the theoretical studies, first for a reflecting object, and then for a transparent object. In [32], from the model of scattering reflecting object discussed in Section 3.1, a problem concerning speckle dynamics in the image plane of a flat surface performs a complex motion. It was supposed that the scattering centers located in plane (xoy) (**Figure 1**) simultaneously (1) move at a low rate toward ox axis, (2) perform periodic motions with the same period and amplitude toward ox axis, and (3) randomly move in space. It was supposed that the difference of irreversible random center displacements $\Delta u_\kappa = \Delta \vec{u}_\kappa \left(\vec{l}_s + \vec{l}\right)$ appear after another cycle of the object oscillation. The averaging time must be equal to the

oscillation period or be divisible by it. For the time-average radiation intensity $\tilde{I}\left(\vec{q}\right)$ at arbitrary point $\vec{q}$ and for normalized temporal autocorrelation function $\eta(t_1, t_2)$ of this intensity, the following was obtained:

$$\tilde{I} = I_1 + I_2 e^{-\sigma^2/2} \cos(x + \alpha), \tag{10}$$

$$\eta(t_1, t_2) = \eta(u_x) \times e^{-k_{11}/2 - k_{22}/2 + k_{12}(t_1, t_2)} \times \cos(\langle x_1 \rangle - \langle x_2 \rangle), \tag{11}$$

where I_1, I_2, α are constants, x and σ^2 are the mean value and variance of Δu_κ, respectively, obtained by averaging over the time T_1 and over the region with a radius $\Delta x = 2a_s$. This area is located in the vicinity of the point that conjugates the point $\vec{q}$. Function $\eta(u_x)$ is a normalized temporal autocorrelation function corresponding to a translational displacement of object toward ox axis; u_x is value of displacement. Values k_{11}, k_{22}, k_{12}, $\langle x_1 \rangle$, $\langle x_2 \rangle$ have the same meaning as in formula (6). However, now they are parameters characterizing random wave pair phase differences averaged by time T_1.

A similar problem concerning speckle dynamics in the image plane of a transparent object was solved in [37]. An optical system presented in **Figure 2** was discussed. It was supposed that object 3, located near thin diffuser 2, is a thin transparent plate whose lateral surfaces are parallel to plane (x,y). As in the previous case, the discussion was about the complex motion of the plate consisting of (1) its translational low-rate motion along ox axis, (2) its periodic motion toward ox axis, and (3) random small variation of the optical thickness of the plate. The formula for time-average intensity coincided with formula (10), and the formula for the temporal autocorrelation function of this intensity was determined by the expression:

$$\eta(t_1, t_2) = [e^{-k_{11}/2 - k_{22}/2 + k_{12}(t_1, t_2)} \times e^{-\tilde{k}_{11}/2 - \tilde{k}_{22}/2 + \tilde{k}_{12}(t_1, t_2)}] \times \cos(\langle x_1 \rangle - \langle x_2 \rangle + \langle \tilde{x}_1 \rangle - \langle \tilde{x}_2 \rangle). \tag{12}$$

Now, in formula (12), the value x is a wave pair phase difference averaged by time and region with diameter Δx, whose changes are determined by variations of the optical thickness of the plate using formula (9). Parameters k_{11}, k_{22}, k_{12}, $\langle x_1 \rangle$, $\langle x_2 \rangle$ in formulas (11) and (12) have the same meaning. Parameters $\tilde{k}_{11}$, $\tilde{k}_{22}$, $\tilde{k}_{12}$, $\langle \tilde{x}_1 \rangle$, $\langle \tilde{x}_2 \rangle$ are similar to values k_{11}, k_{22}, k_{12}, $\langle x_1 \rangle$, $\langle x_2 \rangle$, but they are the parameters of the speckle dynamics emerging due to the roughness of the plate performing a translational motion.

If the roughness is homogeneous, i.e., $\tilde{k}_{11} = \tilde{k}_{22}$, $\langle \tilde{x}_1 \rangle = \langle \tilde{x}_2 \rangle$, then instead of (12), we have:

$$\eta(t_1, t_2) = \eta(u_x) \times e^{-k_{11}/2 - k_{22}/2 + k_{12}(t_1, t_2)} \times \cos(\langle x_1 \rangle - \langle x_2 \rangle), \tag{13}$$

where

$$\eta(u_x) = e^{-\tilde{k}_{11} + \tilde{k}_{11}\rho_{12}(u_x)} \tag{14}$$

is a normalized temporal autocorrelation function of radiation intensity corresponding to the translational motion of the plate, and $\rho_{12}(u_x)$ is a normalized temporal autocorrelation function of phase difference of wave pairs changing in time as a result of movement of a rough transparent plate.

Let us note that the theory of dynamics of time-averaged speckles in the image plane of a thin transparent object in the absence of its displacement and oscillation was discussed in [36].

3.4 Discussion of theoretical results

Therefore, if translational motion of a reflecting or transparent object is absent, the averaging time is divisible by the cyclic loading period, and there are no irreversible deformations in the object, then, according to Eqs. (9)–(11), the observer in the image plane will see a pattern of averaged speckles invariable in time. If irreversible processes that alter the optical paths of the waves emerge in a small region of the object at some phase of oscillation, then the speckle pattern in the conjugated region will change. As the formulas for normalized autocorrelation functions (6) and (11) at $\eta(u_x) = 1$ coincide, the pattern of averaged speckles can be regarded as a speckle pattern of some stationary object. In case of the emergence of irreversible processes that alter the shape of the reflecting object at the structural and/or macroscopic level, or the density of the transparent object, the speckle pattern of such a "stationary" object will vary.

For the reflecting object, value x in the cosine input is proportional to the displacement difference of surface points $\Delta u = \Delta \vec{u} \left(\vec{l_s} + \vec{l} \right)$ located at some characteristic (mean) distance Δx. If the deformation variance is small ($k_{11}, k_{22} \to 0$), then values $\tilde{I}$ and η in the above formulas will depend on Δu by the law of cosines. Thus, the formulas go into the ratios known in the shear variants of holographic, correlation, and dynamic speckle interferometry. Let us note that there emerges a potentiality to determine the components of vector $\Delta \vec{u}$ by means of recording and procession of speckle images recorded simultaneously at different directions of the object illumination or observation.

4. Experiment

4.1 Dynamic speckle interferometry of flat specimens in periodic bending

In our first experiment, the results of theoretical analysis presented in Section 3.1 were applied to study fatigue phenomena emerging in high-cycle fatigue of medium-carbon steel 50 [34]. The scheme of specimen loading is presented in **Figure 3**; the dimensions and shapes of the specimen as well as the speckle image of the control area are shown in **Figure 4**. Before testing, the sample was subjected to fine grinding and annealing. A 2 mm thick flat specimen was loaded with 50 Hz frequency; the number of cycles reached 1,200,000; and maximum cycle amplitude $\sigma_{\max}$ varied from 0.2 to 0.82 σ_{02}, where σ_{02} is the flow limit of steel 50. The surface area near the maximum stresses was illuminated by a laser module with wavelength $\lambda = 655$ nm and 20-mW power. Speckle images with magnification m = 0.1 were captured at a certain phase of the object oscillation and entered into a computer with a frequency about 10 Hz. The minimum speckle size $2b_s$ in the object image plane equaled 40 μm. Films of 20- to 60-s duration were recorded at various stages of specimen testing. To determine value η that is involved in formula (7), we took digital values of intensity at one point (pixel), but at different time points t_1 and $t_1 + \tau$. The digital value of intensity $I_1(t_1)$ corresponded to the beginning of the film, and $I_2(t_1 + \tau)$ corresponded to a frame at time point $(t_1 + \tau)$. A part of the surface size $2a_s = 2b_s/m$ was regarded as one "object" of the object ensemble. It was supposed that this "object" was located in the vicinity of a point conjugated to the pixel we are discussing. The array of the areas' size $2a_s$ located in surface area size 1×4 mm (1 and 4 mm along axes x and y, respectively) was regarded as an object ensemble. Measurement of η was determined by formula:
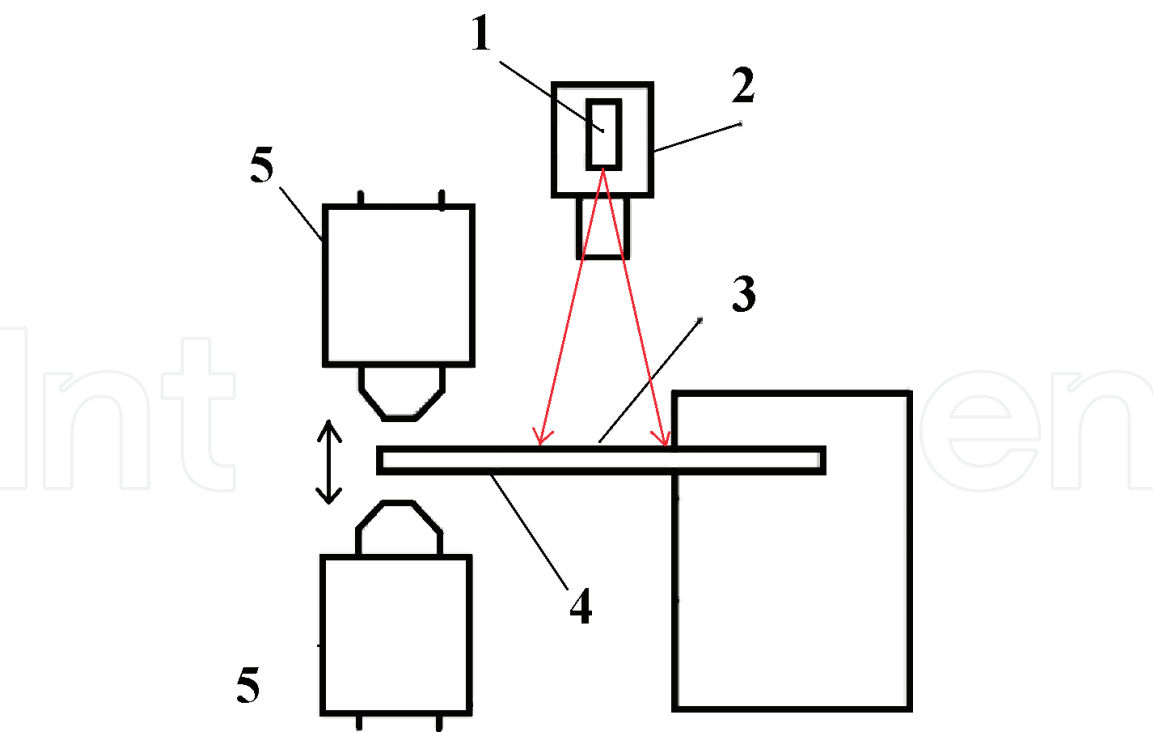
Figure 3.
Scheme of periodic bending: 1—laser module, 2—TV camera, 3—control zone, 4—specimen, and 5—electromagnet.
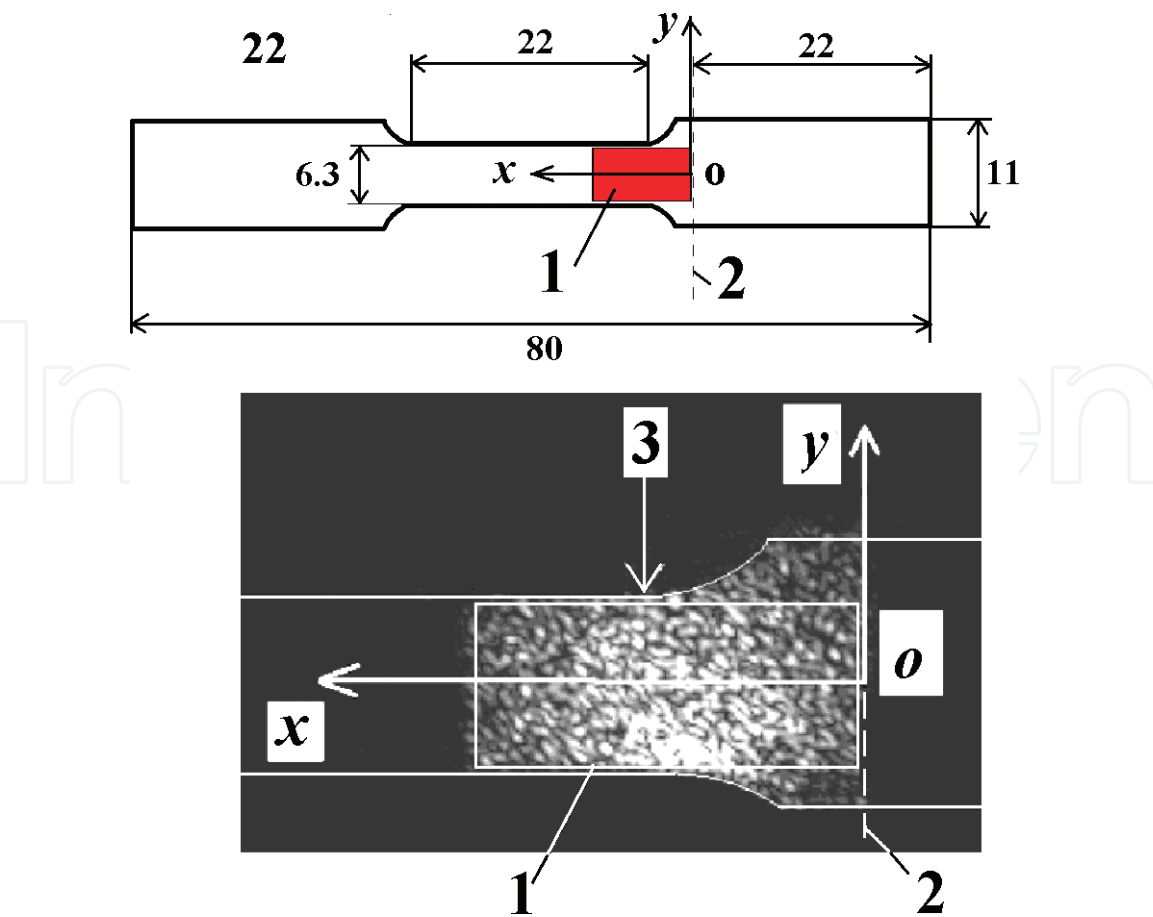

Figure 4.
Dimensions and shape of the specimen (top) and speckle pattern (bottom): 1—control zone, 2—clamp line, and 3—maximum stress spot.

$$\eta(\tau) = \frac{\langle [I_1(t_1) - \langle I_1(t_1)\rangle][I_2 - \langle I_2(t_1 + \tau)\rangle]\rangle}{\sigma_1 \times \sigma_2} \tag{15}$$

where the angle brackets denote arithmetic mean values in the named object ensemble, and σ_1 and σ_2 are standard deviations of values $I_1(t_1)$ and $I_2(t_1 + \tau)$.

Figure 5 presents a typical dependencies $\eta = \eta(\tau)$ obtained early in the fatigue testing experiment at $\sigma_{max} = 0.4\sigma_{02}$. The dark spots denote the experiment; and the dashed line denotes a Gaussian autocorrelation function. The deviation of the experimental data from the theory is in the 5% range. As is seen from the graphs, the autocorrelation function declines from 1 to the fixed level $\eta^* = 0.83$. According to our theory, the decline of value η and leveling-off are the indicators of homogeneity and stationarity of random process $\Delta u = \Delta u(t)$ discussed in Section 3.1. As the directions of illumination and observation are close to the surface normal, $\Delta u = \Delta \vec{u}\left(\vec{l_s} + \vec{l}\right) \cong 2\Delta u_z$, where Δu_z is the projection of vector $\Delta \vec{u}$ on the surface normal. Using the surface decline on 1/e to level η^*, we obtain that the intensity fluctuation correlation time is 7 s. One can accept that this time rivals with relaxation time τ_0 of random value Δu_z, or difference of the displacement of two surface points toward the normal. These points are located in a 400-μm area. From formula $\eta^* = \exp[-k_{11}] = \exp\left[-(2\pi/\lambda)^2 4\sigma_{\Delta u_z}^2\right]$, we obtain that standard deviation $\sigma_{\Delta u_z}$ of values Δu_z equals to 23 nm.

Analysis of the experimental data obtained in the sections of stationary surface relief variations showed the following. When σ_{max} varies from $0.2\sigma_{02}$ to $0.82\,\sigma_{02}$, correlation time τ_0 of relative displacements Δu_z varies from 60 s to values of the 10^{-1}-s order. At the same time, when σ_{max} varied in the named range, value $\sigma_{\Delta u_z}$ stayed practically invariable, at the 5-nm level on the average. Rare measurement lunges of $\sigma_{\Delta u_z}$ from 10 to 20 nm were observed.

In many cases, we recorded very complex dependences $\eta = \eta(\tau)$. Their analysis enabled us to suppose that they corresponded to several processes occurring simultaneously and altering the phases of scattered waves at different rates. Because of difficulties in the interpretation of such data, the technique was upgraded. A theory of time-averaged speckles discussed in Section 3.3 was proposed. Applications of the results of this theory are discussed in the next section.
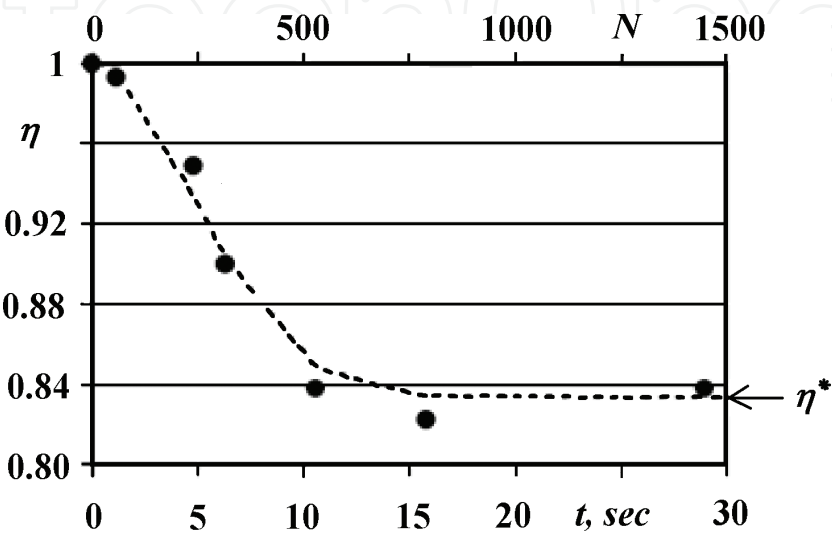

Figure 5.
Temporary autocorrelation function of intensity fluctuations due to metal fatigue: •—experiment and ---- theory.

4.2 Application of time-averaged speckles

We used the technique of time-averaged speckles to study the micro- and macro-variations of the surface shape in high-cycle fatigue of constructive and model materials. The main objective of the conducted research work was to clear up the matter of what happens in the material during crack initiation.

Beams made from pipe steel 09Г2С loaded by three-point bending were used in the experiment. The shape and dimensions of the specimens as well as the position of the bumps are presented in **Figure 6**. A Charpy notch was made in the beam to localize the crack initiation spot. The surface of the beams was subject to fine grinding, and then they were annealed in vacuum. After annealing, the surface of some specimens was polished. After polishing, roughness parameter R_a was in the 1- to 50-nm range. Let us note that for both polished and unpolished specimens, we observed the same results in a qualitative sense.

The specimens were tested in a resonance-type machine of MIKROTRON (RUMUL) type with near-100 Hz frequency and a 0.1 load ratio. The value of the maximum force exerted (1.1 kN) was selected experimentally from the condition of emergence of a 0.1-mm long crack after hundreds of thousands of loading cycles. Variation of resonance frequency by 10% usually preceded the emergence of a crack of this length.

The scheme of the optical setup applied for recording of the average speckle images is presented in **Figure 7**. The optical setup was located on the platform of the testing machine. Object 4 was illuminated by beam 2 from laser module 1 of a KLM-H650-40-5 type with the wavelength of 0.65 μm and 40-mW power. As speckles do not emerge when a mirror surface is illuminated, mat glass 3 was put into the lighting beam to form speckle fields when specimens with the polished surface were tested. The speckle image was recorded in the specimen image plane. The magnification of the optical system equaled 0.7. The diaphragm size of lens 5 was selected so that the minimum speckle size slightly exceeded that of a photocell in the photocell array of the TV camera 6. A monochrome VIDEOSCAN-415M-USB TV camera with an array containing 782×582 photocells of 8.3×8.3 μm size was used in the experiments. Averaging time T_1 equaled 50 oscillation periods. We supposed that in the most damaged surface area, this time exceeded the correlation time of wave pair phase difference τ_0 which is equal to 0.1 s.

Figure 8 presents distribution of correlation coefficient η found by two 8-bit digital speckle images of the specimen.
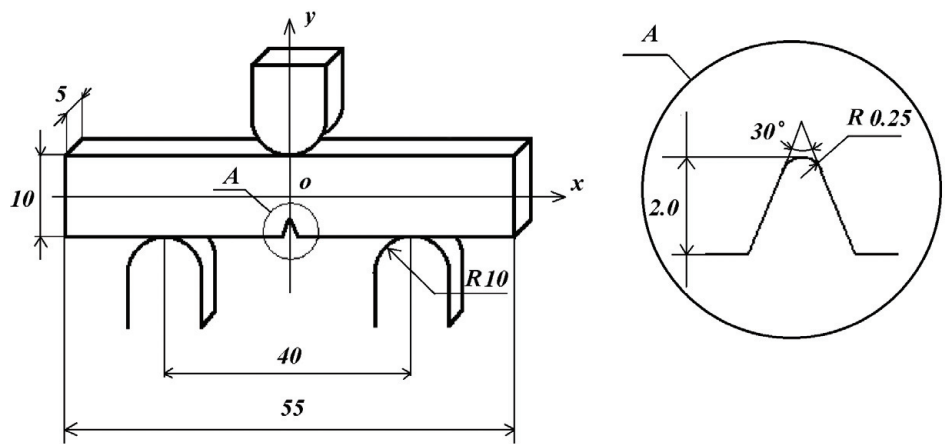

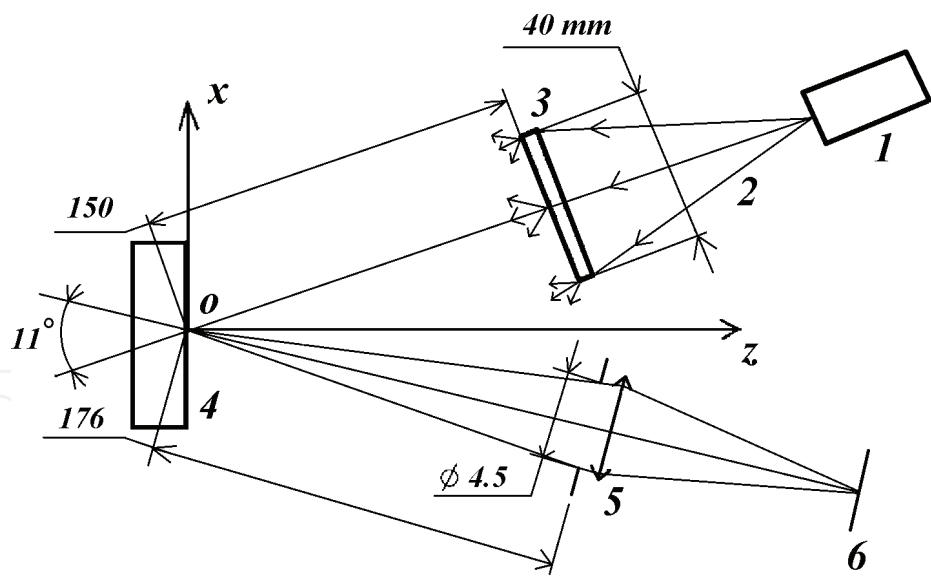
Figure 6.
Shape and dimensions of the specimen.

Figure 7.
Scheme of the optical setup. 1—laser module, 2—illuminating radiation, 3—mat glass, 4—specimen, 5—lens with diaphragm, and 6—photosensor array of the TV camera.
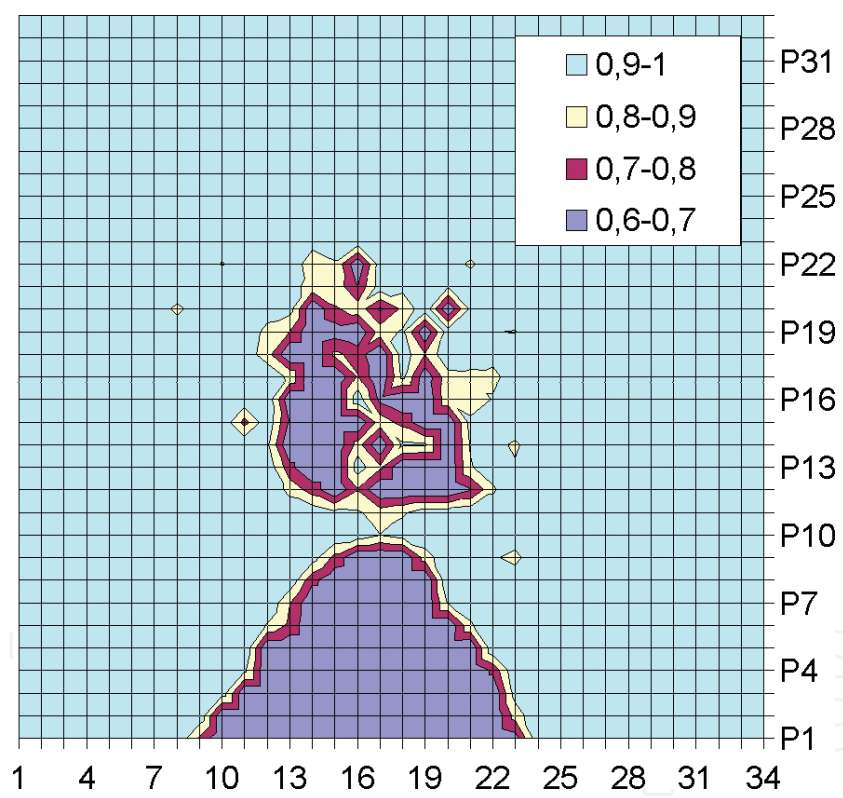

Figure 8.
Distribution of correlation coefficients η found in a 4 × 4-pixel section.

The first image was obtained at loading cycle number N_1 equal to 57,000, and the second image was obtained at cycle number N_2 = 92,000. Speckle field variations started at N_2 equal to 72,000 cycles. Value η was found using formula (15).

Figure 9 presents three-dimensional surface profiles near the notch at N_1 = 57,000 and N_2 = 92,000. The profiles were recorded using an optical profilometer WYKO NT-1100 with a 3-nm height measuring error.

As it is seen from **Figure 9**, at 92,000 cycles, two zones emerged in front of the notch. The first zone is a pitch about 0.5 μm deep with the diameter of 500 μm. The pitch center was at the distance of about 250 μm from the notch tip. Besides, a second small zone of about 50 × 100-μm size where a fatigue crack initiated
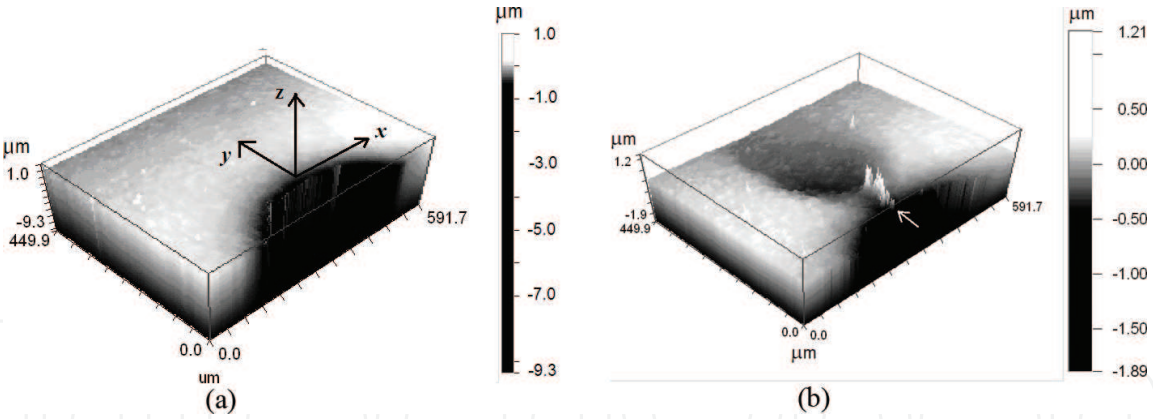
Figure 9.
Surface profiles: (a) at 57,000 cycles and (b) at 92,000 cycles.

emerged immediately at the notch tip. This area is shown by an arrow in **Figure 9b**. This zone consisted of irregularities of 5- to 1-μm transverse size and the height of scores of nanometers.

Figure 10 presents joint graphs showing altered relief heights Δh and correlation coefficient variation η in the pitch image plane along ox axis.

The scan line of the profilometer passed through the pit center, and value η was determined using formula (15) by scanning of a 4×4 pixel-size section. It is seen from the picture that the maximum variations of value η fall on the steepest surface slopes in the pit. Minimum variations of value η correspond to the sections beyond the pit and at its bottom.

Comparison of surface shape variation within the pit with variations of value η in the conjugated region showed that these variations agree with formula (11). The mean value of the scattering center displacement difference at the bottom of the pit can be accepted as zero. In this case, in formula (11), variation of value η will be determined by the parameters contained in the exponent. Values $[\lambda/(4\pi)]\sqrt{-\ln(\eta)}$ corresponding to the bottom of the pitch equaled several nanometers which corresponded to the profilometer data. In **Figure 11**, for five scan lines, black dots show dependence of value η that falls on the steepest slopes of the surface, from the
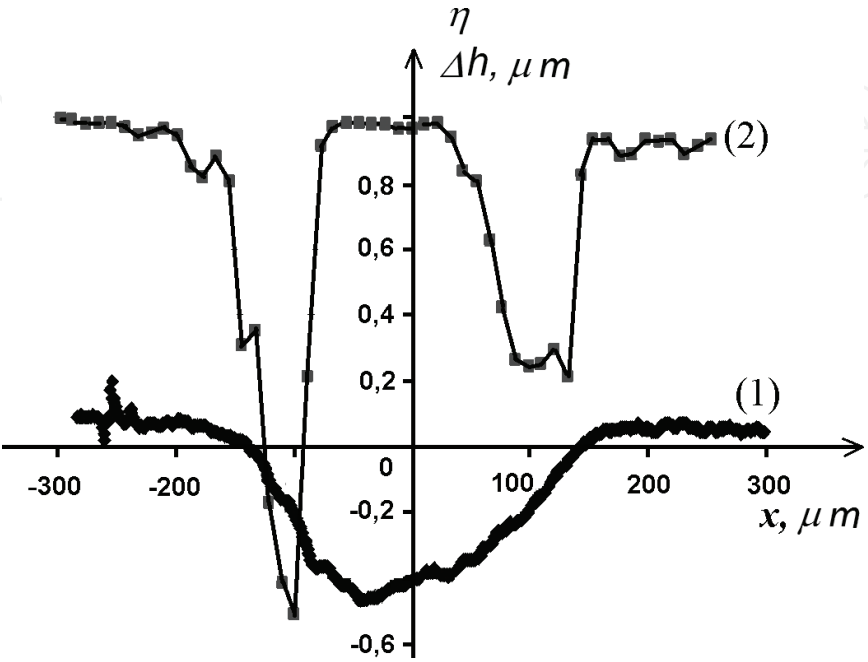

Figure 10.
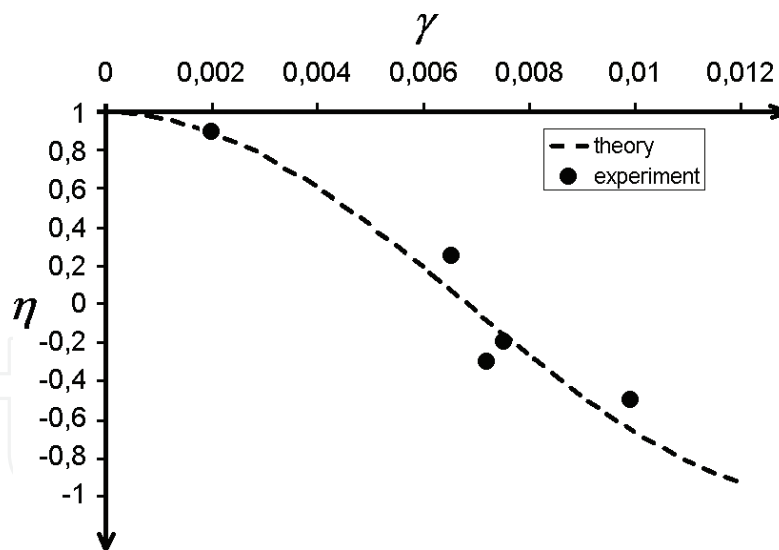*Joint dependences (1) $\Delta h(x)$ and (2) $\eta(x)$.*

Figure 11.
Theoretical (—) and experimental (•) dependences $\eta(\gamma)$.

maximum measurement of the surface profile slope ratio γ. The latter value was found by the surface profile in the graph. The dotted line corresponded to formula (11), in which it was accepted that $\langle x_1 \rangle = 0$ and $\eta(u_x) = 1$; the exponent was substituted by 1 and the cosine argument was $(4\pi/\lambda)\gamma 2x_s$, where $2x_s$ is the size of the surface area equal to the linear resolution of the lens (12 μm). As seen from **Figure 11**, we have fairly good coincidence of the theory and experiment.

As seen from **Figure 9**, about half of the crack formation region lies within the pit, and the other half is beyond the pit. For the latter section, the measurement of η equaled 0.8. Suppose in (11) if the cosine equals 1, $\eta(u_x) = 1$, and $k_{11}, k_{12} = 0$, we obtain that the roughness parameter R_a variation equals 20 nm.

The measurement of R_a was determined by the equation $R_a \cong 0.8\lambda\sqrt{-2\ln\eta}/[2\pi(l_{sz} + l_z)]$, which is fair if the relief heights are distributed by the Gaussian law. Here, l_{sz} and l_z are the projections of unit vectors $\vec{l_s}$ and $\vec{l}$ on axis z, respectively, and $l_{sz} = l_z = 0,98$.

According to the profilometer data, variation of value R_a in the segment equaled 25 nm.

Figure 12 presents typical dependences of $\eta(N)$ that correspond to five surface sections of another specimen. The graph numbers coincide with the section numbers. The fatigue test conditions for this specimen did not differ from those for the previous one; the test was stopped only after the crack initiation and a small increase in its length.

Analysis of three-dimensional profiles of the surfaces of two specimens showed that they were the same in the qualitative sense. The surface spots for plotting of dependences $\eta(N)$ in **Figure 12** were selected so that they could clear up the emergence order of the two above zones at the notch tip. This information can be beneficial for creation of crack initiation physical models. Section 1 was selected beyond the contraction; sections 2 and 3 were selected on the path of the motion of the plasticity zones in front of the crack. Section 4 was located at the very notch tip, and section 5 was taken on the contraction edge on the line approximately passing through its center parallel to the specimen axis. The decrease of value η from 1 to 0.95–0.97 for section 1 at the end of the experiment is caused by the hardware noises and partially by slight translational motion due to degradation of the material. The centers of sections 2 and 3 rivaled, but their size differed. Section 2 of 22×22-μm size consisted of four regions of $\Delta x = 11$-μm size, and in section 3, there were 16 such regions. It is evident that dependences $\eta(N)$ for these two sections
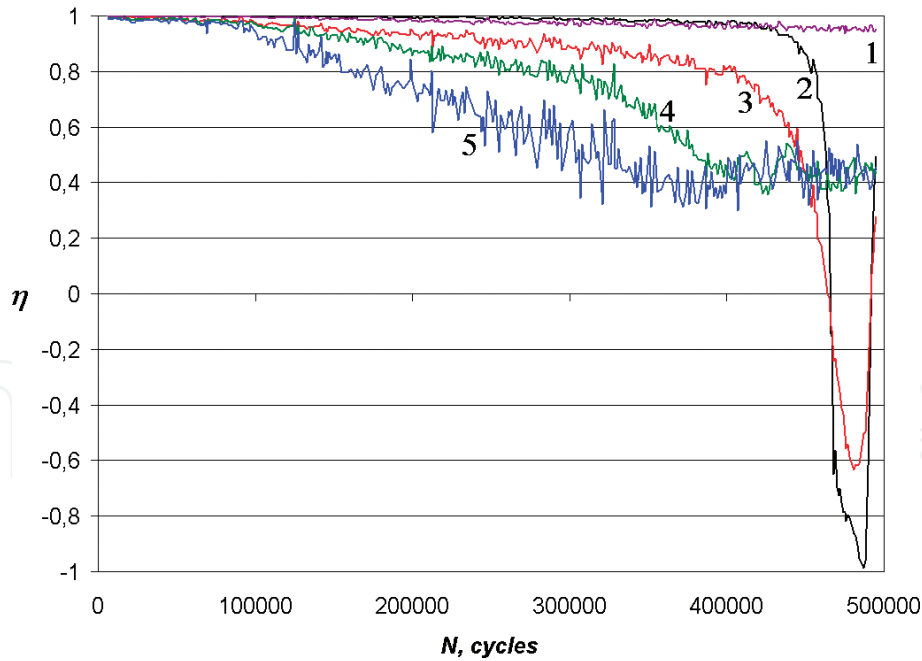
Figure 12.
Dependences η(N) corresponding to five sections of the surface: 1—section of 44 × 44-μm size at the distance of 640 μm from the notch tip. 2—section of 22 × 22 μm size at the distance of 180 μm, 3—section of 44 × 44-μm size at the distance of 180 μm, 4—section at the notch tip of 44 × 44-μm size, 5—section of 44 × 44-μm size on the slope of the contraction.

twice arrive at zero nearly simultaneously; however, their minimum measurements differ. For section 2, value a η nearly reaches -1, and for section 3 the minimum measurement equals -0.62. From the viewpoint of our theory, in compliance with formula (11) reaching -1 by value η means its dependence on $\langle \Delta u_z \rangle$ by the law of cosines with amplitude $\exp(-k_{22})$ equaling 1 ($k_{22} = 0$), and values $k \times 1.96 \times \Delta\gamma \times \Delta x / \lambda$ in every small region of 11-μm size reach value $\pi/2$. Let us take value $\Delta\gamma$ that characterizes a rigid surface rotation for the measure of plastic deformation on the 11-μm base. Then it follows from our analysis that at $\eta = -1$, a homogeneous plastic surface deformation equaling 7.5×10^{-3} occurs in section 2. For section 3 amplitude, $\exp(-k_{22})$ equals 0.62. Thus, we get that the plastic deformations in section 3 of 44 × 44-μm size are inhomogeneous, and the standard deviation of values $\Delta\gamma$ from 7.5×10^{-3} equals 3.3×10^{-3}.

It is seen in **Figure 12** that notable deviations of dependences 4 and 5 from the horizontal line start practically simultaneously at 70,000–80,000 cycles. This suggests that the formation of irregularities in the small zone and the contractions probably start simultaneously. Above, it was shown that a decline of value η from 1 to about 0.8 in the conjugated region corresponds to crack initiation at the notch tip. For section 4, such a decline occurred at about 280,000–300,000 thousand cycles. Then, dependence 4 levels off at $N \approx 400,000$. This suggests cessation of irreversible process in section 4 after the crack start and the increase in the crack length. A decrease of value η to 0.45 at 330,000 cycles approximately in linear fashion is characteristic for to section 5. Then dependence $\eta(N)$ also goes to the horizontal section which speaks for the completion of contraction formation.

4.3 Studying fatigue of Plexiglas

The experiments conducted with Plexiglas of "ACRUMA" brand aimed at studying the peculiarities of fatigue damage accumulation in the volume of the specimen shown in **Figure 6**. The specimens were made from a plate 5-mm thick. The protective film preserving the polished surfaces was taken off before the

fatigue test. The equipment shown in **Figure 7** was used to record the speckle images. The specimen was illuminated through mat glass, the sounding waves passed through the specimen. The observation direction was selected either along the normal or at the angle of 30° to the normal. In the latter case, irreversible processes in the depth of the specimen could be controlled by distribution of value η. The three-point bending test under the condition of high-cycle fatigue was run on the machine discussed in the previous section. By now, an article has been prepared on the basis of the obtained data, which is now being reviewed by the editors of an optical magazine. As agreed with the magazine editors, the results of the conducted experiments will be available after publishing. We will only note that we were for the first time able to view in detail the process of transition of originally continuous three-dimensional medium into a destroyed state. Using the formulas in Section 3.3, we evaluated the limiting variations of the refraction index and density prior to fatigue destruction of Plexiglas. The crack initiation processes in steel and Plexiglas were very similar, even coinciding in some details. The difference consists in the fact that metals have the mechanism of energy dissipation connected to dislocation motion. That is why during local plastic deformation, variation of the object shape (emergence of a contraction) can take place. An amorphous material like Plexiglas does not have such a mechanism. That is why plastic deformations come into effect as volume/density variations.

4.4 Dynamic speckle interferometry of intracellular processes

In our early experiments studying the processes occurring inside live cells, we used the formulas discussed in Section 3.2 of the theory. The main long-term objective of the undertaken studies was search of approaches that would permit creation of an optical technique and a device studying the processes in the live cell membranes. The first objective of the experiments was search of cell metabolism parameters. We used an optical setup whose scheme corresponded to the optical scheme discussed in the theory (**Figure 2**). The photo of the setup is shown in **Figure 13**. A semi-conductor laser module with the wavelength $\lambda = 532$ nm and 20-mW power as well as the TV camera discussed above in Section 4.2 were used. The setup was placed into a thermostat that maintained the temperature of 36 ± 0.1°C. A transparent cuvette with two glass supporters in a horizontal position in the nutrient solution was fixed on a small table near the mat glass. The first supporter contained a monolayer of cultured cells; the second one was cell-free. Speckle images of the supporters are shown in **Figure 14**. The light lines in the picture show the typical sections selected for determination of value η using
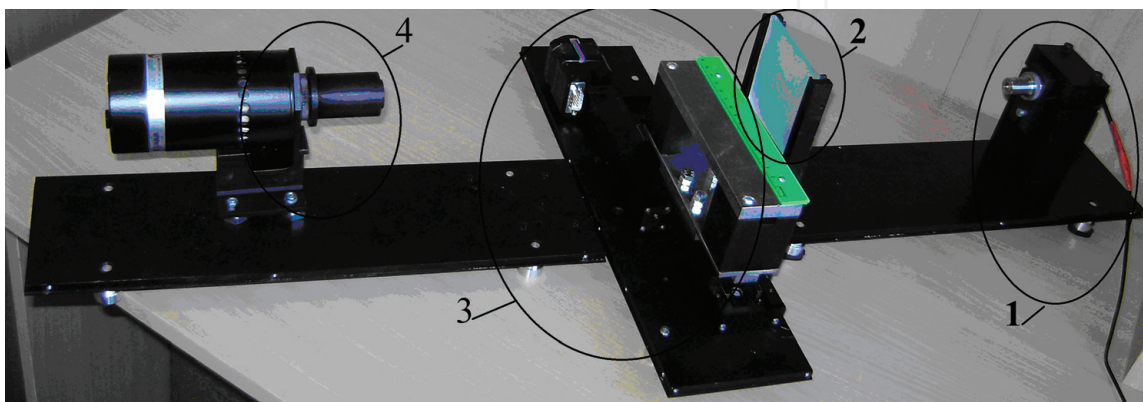

Figure 13.
Photograph of the optical device: 1—laser module with micro-objective, 2—mat glass, 3—lock of the object on the platform of the motorized translator, and 4—camera with lens.
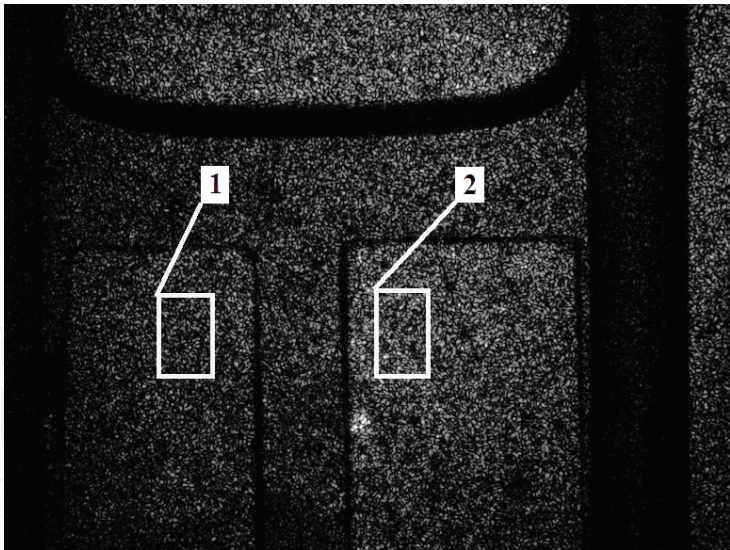
Figure 14.
Speckle images of supports in a transparent cuvette with nutrient solution.

formula (15). The measurements of η were determined using the films recorded during 20–40 s. **Figure 15** presents dependences $\eta(t)$ corresponding to the nutrient solution (top), to the cells in the nutrient solution (middle), and to the herpes simplex-infected cells (bottom). It is seen from the graphs that in all the cases dependence $\eta(t)$ levels off in several seconds. According to the theory, the presence of a constant level speaks for the fact that random radiation intensity variations in the selected image fragment and variations in difference Δu of the optical wave paths in time in the conjugated region are stationary processes. By the measurements of the fixed levels, we determined variances $\sigma^2_{\Delta u}$ of values Δu. In the assumption that random values Δu corresponding to the cells and the nutrient solution are uncorrelated variables, we determined values $\sigma^2_{\Delta u}$ corresponding to the cells.

While processing the films of 20- to 40-s duration recorded for several hours, we detected various types of dependences $\eta(t)$. Along with the graphs similar to those presented in **Figure 15**, we obtained dependences that did not level off as well as graphs that had rather a composite view. All-day graphs of dependences $\sigma_{\Delta u}(t)$ at a 0.5-h pitch were reproducible in about 50% of the cases. Analysis of obtained dependences $\eta(t)$ showed that their complicated character is probably connected to
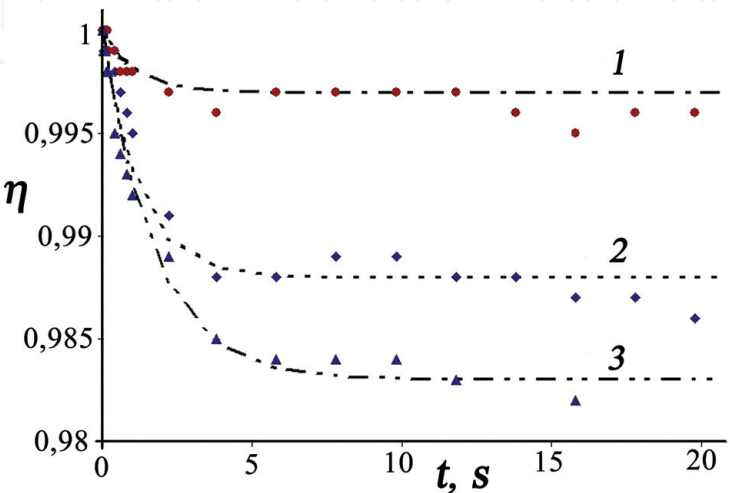

Figure 15.
Dependence $\eta(t)$ corresponding to: 1—nutrient solution, 2—cells in the nutrient solution, and 3—infected cells in the nutrient solution.
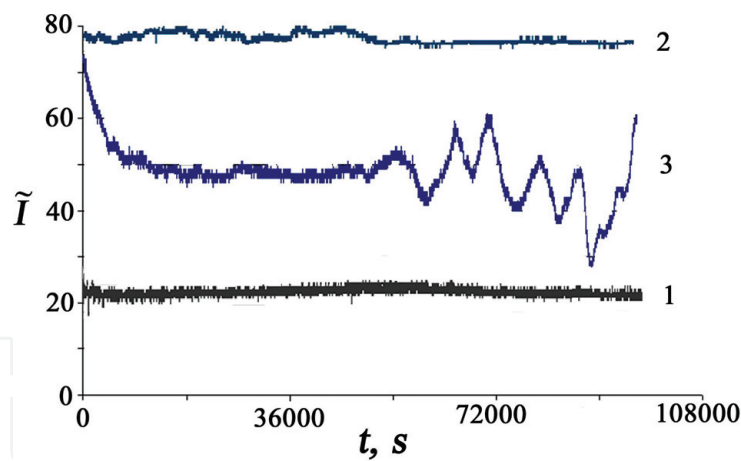
Figure 16.
Dependence of time-averaged intensity Ĩ on time for the pixels corresponding to: 1—nutrient solution, 2—cell, and 3—herpes simplex virus in a cell.

the presence of several processes altering the phases of the sounding waves at different rates. In this regard, we used a time-averaged speckle technique discussed in Section 3.3. Application of this technique enabled us to obtain well-reproducible data. **Figure 16** presents typical dependences of the time-averaged digital value of intensity $\tilde{I}$ corresponding to the nutrient solution, to a cell in the nutrient solution and to a herpes simplex virus-infected cell in the solution. The dependences are taken from our paper [38]. Analysis of the dependences belonging to the latter type showed that variation features of value $\tilde{I}$ well corresponds to the stages of virus development in cells. **Figure 17** presents typical dependences $\eta(t)$ corresponding to the nutrient solution, to the cells in the nutrient solution, and to the herpes simplex virus-infected cells in the nutrient medium.

The shown dependences were well-reproducible when a monolayer of cultured cells of various cell lines was infected with herpes virus.

Figure 18 presents joint dependences of $\sigma_{\Delta u}(t)$ and temperature T on time for L-41 cell line [39]. For the linear correlation coefficient of two arrays $\sigma_{\Delta u}$ and T, we obtained a value equal to 0.88. **Figure 14** shows dependence of $\sigma_{\Delta u}$ on T from our early work [35]. L-41 cell line was also used in the experiment.

As the metabolic processes are manifested more distinctly when the temperature rises, the above data presented in [38] were used to substantiate application of value $\sigma_{\Delta u}$ as the parameter that characterizes the activity of cultured cells.
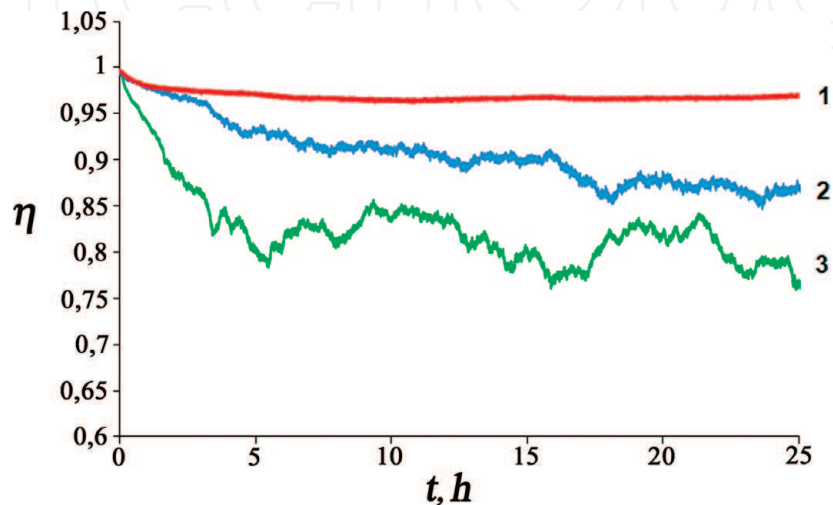

Figure 17.
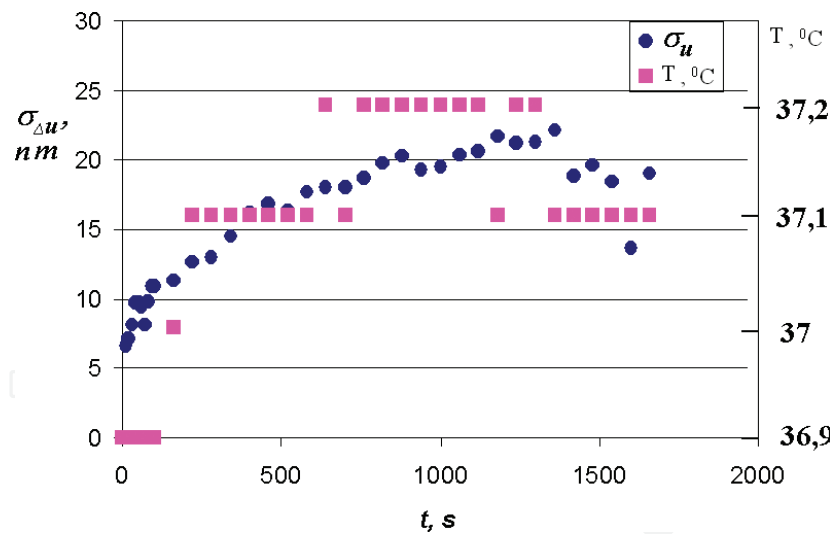*Typical dependence η(t) for Vero line: 1—nutrient solution, 2—virus-free cells, and 3—cells with virus.*

19

Figure 18.
Joint dependence of $\sigma_{\Delta u}$ and temperature on time at small heating rates.
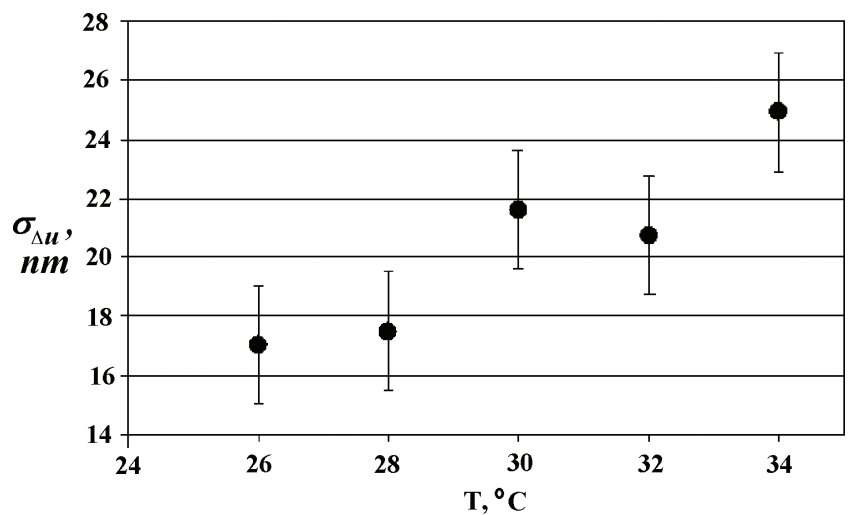

Figure 19.
Dependence of $\sigma_{\Delta u}$ on the temperature.

5. Discussion of results and prospects for further studies

5.1 Studying high-cycle fatigue of metals

The conducted theoretical and experimental research showed that the dynamic variant of speckle interferometry can be used for quantitative evaluation of irreversible displacements and deformations occurring in metals with high-cycle fatigue on the 10-μm order bases. The peculiarity of this evaluation is that application of time-average speckles makes it can be conducted in real time, i.e., without interruption of cyclic deformations (**Figure 19**).

The technique is fairly simple, because it does not require any synchronization of the load value applied to the object and the frame capture moment. It is characterized by high accuracy and sensitivity.

In [32], it was shown that when a 10×10-pixel fragment is selected at the variation of η from 0.3 to 0.99, the ratio error of its determination does not exceed 1%. It was shown that a small error in determination of value η by formula (15) is related to the features of radiation intensity $\tilde{I}$ distribution in the speckle pattern. The record error of value η was found to equal the sum of determination errors of

values $\tilde{I}$ multiplied by 10^{-2}-order coefficients with different signs. The random meaning of the sign was determined by the difference of $\tilde{I}$ in a pixel and by the mean measurement in the image fragment.

High sensitivity of the speckle technique to deformations is based on the phenomenon of multiple-wave interference with the same initial phases. Speckles emerge as the result of multiple-wave interference with random initial phases. So the emergence of multiple-ray interference is in many ways similar to wave interference in a diffraction grid is not evident. This question was briefly discussed in [34, 40]. Because of the significance of the matter, let us dwell upon it. Let there be a great number of point diffusers on the surface in a region of ΔX diameter with the center at point A, and let value ΔX equal the linear resolution of the lens. For certainty, let the surface be illuminated and observed along the normal. The waves with random initial phases going from the scattering centers form random intensity value $\tilde{I}$ at conjugated point A' of image plane. Now let us imagine that a slight plastic rotation around an axis parallel to oy axis. Let the rotation axis be located at the edge of a region with ΔX diameter. Now let us discuss the scattering centers with the following properties: (1) the waves scattered by these centers have the same amplitudes and initial phases, (2) y-coordinates of the centers are random, (3) along ox axis they are located at the same Δx distance. We suppose that such centers will always be found if their number is large. Let Δu_z be the maximum displacement along the normal in the region, and $M = \Delta X/\Delta x$. In [34], we showed that at point A' the radiation intensity will vary in a quasi-periodic mode proportionally to value $\sin^2(2\pi \times \Delta u_{z0} M/\lambda)/\sin^2(2\pi \times \Delta u_{z0}/\lambda)$, where $\Delta u_{z0} = \Delta u_z/M$. Analysis of the obtained expression showed that in deformation of the materials used in practice, the periodicity corresponding to the denominator is difficult to implement. From the numerator period, we obtain that $\Delta u_{z0} \times M = \Delta u_z = \lambda N/2$, where N is the interference period (period of value $\tilde{I}$). The latter ratio is also implied by formulas (6), (10), (11), if in these formulas we accept that $\sigma^2 = 0$, $\langle x_1 \rangle = 0$, and $k_{11}, k_{22} = 0$. Therefore, the multiple-wave interference that we have discussed is equivalent to interference of two waves spreading from the centers located at the opposite edges of the region with ΔX diameter. Expression $\Delta u_{z0} \times M = \lambda N/2$ may be interpreted in a different way. Having accepted that $N = 1$, we have: $\Delta u_{z0} = (1/2)\lambda/M = (1/2)\lambda_0$. We obtain that variation of value $\tilde{I}$ per period may also be interpreted as the variation result of the interference period of two coherent waves with wave length $\lambda_0 = \lambda/M$. This variation appears in a relative displacement of two scattering centers located at distance Δx by value Δu_{z0}. Let us accept the limiting sensitivity Δu_{z0} of the technique, the 1-nm order is theoretically evaluated above and experimentally confirmed in [41]. Then, formally we obtain that value λ_0 is in the X-ray wave range. This way, if the region with ΔX diameter is so small that the macroscopic deformations in it are homogeneous, then the reflected waves with random initial phases form some random hardly variable speckle brightness value, and the waves with the same initial phases are responsible for quasi-periodic intensity variation on the background of this value.

The conducted experiments showed the possibility in principle to determine the limiting roughness parameter variation ΔR_a, of value $\Delta u = \Delta \vec{u} \left(\vec{l_s} + \vec{l} \right)$ for the reflecting object and the refraction index of a transparent object corresponding to the crack start. By monitoring the variation rate of these parameters on the bases of the 10–100 µm order, one can assess the approximate time to macro-fracture. It is noteworthy that in practice, not always is there an opportunity to illuminate the object under control with laser radiation, and the conventional nondestructive testing techniques are poorly adapted for measurement on such bases. The

discussed speckle method could be used as the tool for upgrading of the conventional testing techniques. The technique is convenient for target detection in search of local irreversible deformations and calibration of other techniques.

Fatigue experiments improved understanding of the processes occurring in high-cycle fatigue of materials. For example, the pins that we observed at the notch tip (shown by the arrow in **Figure 9b**) turned out to be pieces of iron carbide. We managed to identify them using Raman scattering [42]. This fact speaks for the significance of heat generation accounting in high-cycle fatigue. The experiments also showed that irreversible processes in the small region close to the notch emerge at the early stages of the fatigue. If inconsistent local deformations emerge at the stage of loading increase, then in arbitrary unloading residual compressive stress must inevitably appear. Thus, the stress and deformation fields at the notch tip will vary considerably with progress of the fatigue. In this context, analysis of not only local plastic, but also of periodically varying elastic deformations is important.

The opportunity for application of the elastic deformation control technique that we have discussed was substantiated in [32]. Deformation $\varepsilon = \Delta u / \Delta X$ of the 10^{-3} order corresponds to values Δu of the 1-nm order and ΔX of the 10-μm order. Plastic deformations 10^{-3} up are more characteristic for most of the conventional constructive materials. If we increase the measurement base by an order, we will proceed into the range of elastic deformations of the 10^{-4} order. It is deformations of this order that emerge in constructions during exploitation. In [43], we conducted a successful pilot model experiment recording values $\tilde{I}$ and η in a specimen under elastic strain. **Figure 20** presents dependences of $\tilde{I}$ and η on the time taken from that paper. The graphs were obtained in periodic deflection of a steel beam. The data correspond to a single oscillation period; the observation and illumination directions selected were not on the surface normal, measurement base ΔX equaled 670 μm. Thus, the approaches that we have discussed are in principle applicable for simultaneous monitoring of both macroscopic elastic deformations on relatively large bases and of local plastic deformations. Development of such techniques can be the subject for further research.
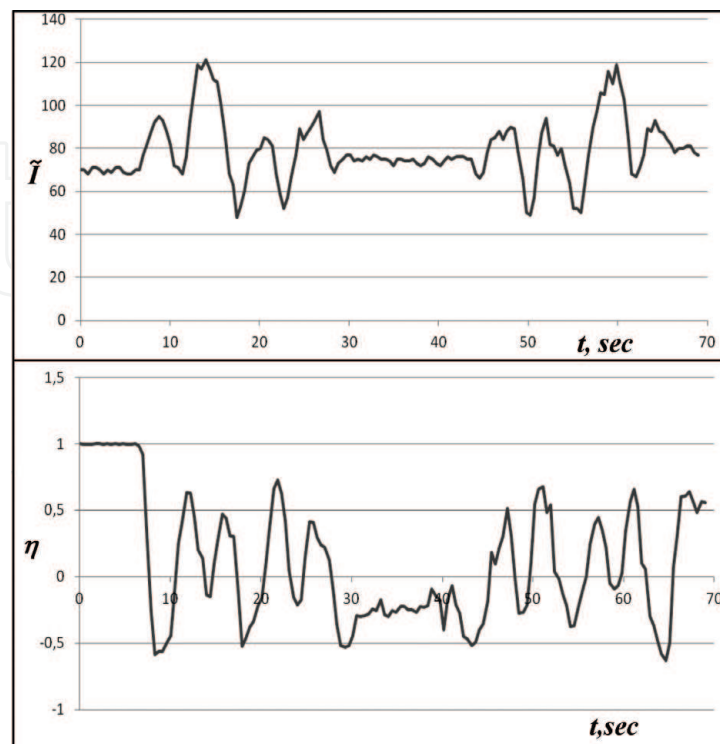

Figure 20.
Dependence of $\tilde{I}$ and η on time in elastic deflection of a steel beam.

The dependence of value η both on the mean value of $x_2 = k\Delta u$ and on its variance k_{22} is the peculiarity of this technique. We managed to obtain numerical values of x_2 and k_{22} for cases $k_{22} = 0$ and $x_2 = 0$, respectively. In [32], it was proposed to obtain the values of $\langle x_2 \rangle$ and k_{22} by simultaneous recording of two speckle images obtained using two lasers. Development of such a technique can be the subject for further research.

In the conducted fatigue experiments, we used an optical system that permits determination mean values, variance, and relaxation time of Δu_z-component of vector $\Delta \vec{u}$. However, the measurements of the above values for other components of vector $\Delta \vec{u}$ are of practical interest. Development of such a technique is the subject of our further research.

5.2 Study of the processes inside live cells

The matters of the accuracy and sensitivity of the technique, the peculiarities of speckle image variations, contribution assessment for values $\langle x_2 \rangle$ and k_{22} to variation of value η discussed in the previous section are fully applied to dynamic speckle interferometry of live cells.

We underpinned and approved a cell activity parameter $\sigma_{\Delta u}^2$, or variance of the difference in the optical path of the cell-sounding waves is such a parameter. However, it is not yet clear what constituents of metabolism affect variation of value $\sigma_{\Delta u}^2$ and to what extent. The study of this problem is the subject of our further research.

Obtaining data by averaging by the cell thickness is a drawback of this technique. Still, the logic of the technique development and the practical needs set the task of determining the mean value, variance, and relaxation time of the medium refraction index in every small section of the cell. The author reported about the ways to solve this problem at two conferences [44, 45]. Theoretical and experimental underpinning of a speckle tomography for the live cell that would permit a solution to this problem is the subject of our further research.

6. Conclusion

This work discussed theoretical and experimental underpinning of an interference technique that permits studying irreversible processes occurring near the surface of reflecting objects and inside thin transparent objects by variation of speckle images. The author's scientific interests lie in the sphere of studying longevity of living and nonliving matter. So, the research targets were specimens made from constructive materials tested for high-cycle fatigue as well as cultured live cells.

The theoretically obtained formulas established the relationship among the parameters characterizing variation of optical wave paths in small sections of an object and the parameters characterizing variation of speckles in the conjugated region. Such parameters for a reflecting object were the mean value, variance, the relaxation time of difference Δu in displacement of scattering centers (points of the surface), time-averaged radiation intensity $\tilde{I}$, and correlation coefficient η for the speckle image fragment taken at the reference and at the current time points. Similar ratios were obtained for a transparent object sounded by multiple waves with random initial phases. The difference consisted of the fact that value Δu was the difference in the optical path of the waves sounding the object.

For the variant, when variation of Δu in time is a random stationary process, we obtained a relation between the normalized spectrum of value Δu and the normalized fluctuation spectrum of $\tilde{I}$.

In experiments set up for testing of the theory, speckle dynamics was created by displacement of a rough transparent plate, by variation of shape, roughness, and the refraction index of metal and Plexiglas specimens in their high-cycle fatigue. Good quantitative coincidence of the theory and the experiment was shown.

It was shown that by way of speckle time-averaging the technique permits real-time determination of the 1-nm-order measurements of Δu on the 10-μm order on bases ΔX, which corresponds to local plastic deformation $\varepsilon = \Delta u / \Delta X$ of the 10^{-3} order.

It was demonstrated that with increasing base ΔX by an order, the technique allows to monitor the variation of elastic macroscopic deformations. So, the possibility, in principle, to use the same technique for monitoring both the deformation field of a part and accumulation of local plastic deformations in an object under periodic strain appears.

It was also shown that using this technique, one can determine the limiting variations of roughness parameter R_a, value ε and refraction index n that correspond to the crack start. Therefore, knowing the limiting measurements of these parameters and monitoring their variation rate while exploiting the part, one could in principle assess the time to its macroscopic fracture. Development of such a technique can be the subject of further research.

When the technique was applied for studying live cells, it was shown that the variance of value Δu can be used as a live cell activity parameter. It was also shown that dependences $\tilde{I}(t)$ and $\eta(t)$ for virus-infected and virus-free cells differ considerably. Modification of this technique for determination of the average measurement, variance, and relaxation time of the refraction index in small areas of the live cell can be the line of further research.

Acknowledgements

Author details

Alexander Vladimirov
Ural Federal University, Yekaterinburg Institute of Virus Infections, Yekaterinburg, Russia

*Address all correspondence to: vap52@bk.ru

IntechOpen

References

[1] Anisimov VI, Kozel SM, Lokshin GR. Space-time statistical properties of the coherent radiation scattered by a moving diffuse reflector. Optics and Spectroscopy. 1969;**27**(3):483-491

[2] Yoshimura T. Statistical properties of dynamic speckles. JOSA. 1986;**A3**(7): 1032-1054

[3] Yamaguchi I. Speckle displacement and decorrelation in the diffraction and image fields for small object deformation. Optica Acta. 1991;**28**: 1359-1376

[4] Aleksandrov EB, Bonch-Bruevich AM. Investigation of surface strains by the hologram technique. Soviet Physics-Technical Papers. 1967;**12**: 258-265

[5] Leendertz JA. Interferometric displacement measurement on scattering surfaces utilizing speckle effect. Journal of Physics E: Scientific Instruments. 1970;**3**:214-218

[6] Vladimirov AP, Mikushin VI. Interferometric determination of vector components of relative displacements: Theory and experiment. Proceedings of SPIE. 1999;**3726**:38-43

[7] Fomin NA. Speckle Photography for Fluid Mechanics Measurements. Berlin: Springer-Verlag; 1998. 219p

[8] Romanov AN. Razrushenie pri Malotsiklovom Nagruzhenii [Fracture in Low-Cycle Loading]. Moscow: Nauka; 1988. 282p; (rus)

[9] Ellyin F. Fatigue damage, crack growth life prediction. London: Chapman and Hall; 1997. 483p

[10] Brinckmann S. On the role of dislocations in fatigue crack initiation [Dissertation]. Groningen, The Netherlands: University of Groningen; 2005

[11] Novikov II, Yermishin VA. Fizicheskaia Mehanika Realnyh Materialov [Physical Mechanics of Real Materials]. Moscow: Nauka; 2004. 328p; (rus)

[12] Lasar J, Hola M, Cip O. Differential interferometry for real-time measurement in high cycle fatigue metal testing. Book of abstracts. In: Conference on PhotoMechanics 2015. 25–27 May 2015. Delft, Netherlands. pp. 64-65

[13] Gough HJ. Fatigue of Metals. London: Benn; 1926

[14] Ustalost metallov. Sbornik statei pod red, G.V. Uzhika [Metal fatigue. Collected papers ed. By G.V. Uzhik]. Moscow: Izd-vo inostr.lit. – Moscow, 1961. 378 p. (rus)

[15] Ivanova VS, Terentiev VF. Priroda Ustalosti Materialov [The Nature of Metal Fatigue]. Moscow: Metallurgija; 1975. 456p; (rus)

[16] Taylor D. The Theory of Critical Distances. Amsterdam: Elsevier; 2007. 307p

[17] Manson SS. Fatigue: A complex subject—Some simple approximations. The William M. Murray Lecture. Experimental Mechanics. 1965;**5**(7): 193-226

[18] Schijve J. Fatigue of structures and materials in the 20th century and the state of art. International Journal of Fatigue. 2003;**25**(8):679-702

[19] Terentiev VF. Ustalost Metallicheskih Materialov [Fatigue of Metallic Materials]. Moscow: Nauka; 2002. 248p; (rus)

[20] Gilanyi A, Morishita K, Sukegawa T, Uesaka M, Miya K. Magnetic non-destructive evaluation of fatigue damage of ferromagnetic steels for nuclear fusion energy systems. Fusion Engineering and Design. 1998;**42**:485-491

[21] Gorkunov ES, Savray RA, Makarov AV, Zadvorkin SM. Magnetic techniques for estimating elastic and plastic strains in steels under cyclic loading. Diagnostics, Resource and Mechanics of Materials and Structures. 2015;**2**:6-15

[22] Tupikin DA. Thermoelectric method of fatigue phenomena control. Control Diagnostika. 2003;**11**:53-61. (rus)

[23] Ignatovich VN, Shmarov SS, Yutskevich SR. Features of formation of deformation relief on the surface of the alloy D16AT fatigue. Aviatsionno-Kosmicheslaiia Tehnika i Tehnologiia. 2009;**67**(10):132-135. (rus)

[24] Yermishkin VA, Murat DP, Podbelskiy VV. Application of photometric analysis of structural images to assess fatigue resistance. Avtomatizatsija i Sovremennije Tehnologii. 2008;**2**:11-21. (rus)

[25] Plehov OA, Panteleiev IA, Leontiev VA. Features of heat release and generation of acoustic emission signals during cyclic deformation of Armco-iron. Fizicheskaija Mezomehanika. 2009;**12**(5):37-43. (rus)

[26] Marom E. Holographic Correlation. In: Erf PK, editor. Holographic Nondestructive Testing. New York: Academic Press; 1974. p. 149-180

[27] Marom E, Muller RK. Optical correlation for impending fatigue failure detection. International Journal of Nondestructive Testing. 1971;**3**:171-187

[28] Kozubenko VP, Potichenko VA, Borodin YS. Study of metal fatigue by speckle-correlation method. Problemy Prochnosti. 1989;**7**:103-107. (rus)

[29] Vladimirov AP. Dinamika speklov v ploskosti izobrazhenija plasticheski deformiruiemogo ob'ekta. Diss… cand. fiz.-mat. nauk [Speckle dynamics in the image plane of the deformed object] [Dissert. Cand. Sci]. Sverdlovsk; 1986. 106p; (rus)

[30] Vladimirov AP. Dinamicheskaia spekl-interferometrija deformiruiemyh ob'iektov. Diss… dokt. tehn. nauk [Dynamic speckle interferometry of deformed objects] [Dissert. Doc. Eng. Sci.] Yekaterinburg; 2002. 393p; (rus)

[31] Vladimirov AP. Dynamic speckle interferometry of the microscopic processes. Proceedings of SPIE. 2012;**8413**:841305; 1-6

[32] Vladimirov AP. Speckle metrology of dynamic macro- and micro-processes in deformable media. Optical Engineering. 2016;**55**(12):121727; 1-10. DOI: 10.1117/1.OE.55.12.121727

[33] Vladimirov AP, Druzhinin AV, Malygin AS, Mikitas' KN. Theory and calibration of speckle dynamics of phase object. SPIE Proceedings. 2012;**8337**: 8337OC; 1-15

[34] Vladimirov AP. Dynamic speckle – Interferometry of micro-displacements. AIP Conference Proceedings. 2012;**1457**: 459-468

[35] Malygin AS, Bebenina NV, Vladimirov AP, Mikitas' KN, Bakharev AA. A speckle_interferometric device for studying the cell biological activity. Instruments and Experimental Techniques. 2012;**55**(3):415-418

[36] Vladimirov AP. Dynamic speckle interferometry of microscopic processes in thin biological objects. Radiophysics and Quantum Electronics. 2015;**57**(8): 564-576

[37] Vladimirov AP. Dynamic speckle interferometry of high-cycle material fatigue: Theory and some experiments. AIP Conf. Proc. 2016;**1740**:040004. DOI: 10-1063/14962663

[38] Vladimirov AP, Bakharev AA. Dynamic speckle interferometry of thin biological objects: Theory, experiments and practical perspectives. In: Banishev AA, Bhowmick M, Wang J, editors. Optical Interferometry. Rijeka, Croatia: InTech; 2017. pp. 103-141. Print ISBN: 978-953-51-2955-4; Online ISBN: 978-953-51-2956-1

[39] Mikhailova YA, Vladimirov AP, Bakharev AA, Sergeev AG, Novoselova IA, Yakin DI. Study of cell culture reaction to temperature change by dynamic speckle interferometry [Electronic resource]. Rossijskij Zhurnal Biomehaniki. 2017;**21**(1):64-73

[40] Vladimirov AP, Kamantsev IS, Veselova VE, Gorkunov ES, Gladkovskii SV. Use of dynamic speckle interferometry for contactless diagnostics of fatigue crack initiation and determining its growth rate. Technical Physics. 2016;**61**(4): 563-568

[41] Vladimirov AP, Kamantsev IS, Ishchenko AV, Gorkunov ES, Gladkovskii SV, Zadvorkin SM. The study of the process of nucleation of fatigue cracks by changing the surface topography of the sample and its speckle images. Deformatsija i Razrushenije Materialov. 2015;**1**:21-26

[42] Tihonova IN, Men'shchikova AA, Vladimirov AP, Ponosov YS, Kamantsev IS, Drukarenko NA, Ishchenko AV. Kompleksnoie izuchenie mnogotsiklovoi ustalosti stali metodami dinamiki speklov, opticheskoi profilometrii, konfokal'noi, skaniruiiushei, magnitnoi I ramanovskoi mikroscopii, XXX Mezhdunarodnaia shkola-simposium po golographii, kogerentnoi optike I fotonike: Materialy shkoly-simposiuma.

Pod red. kand. fiz.-mat. nauk I.V. Alekseienko [In-depth study of high-cycle fatigue of steel using speckle dynamics, optical profilometry, confocal, scanning, magnetic and Raman microscopy. In: XXX International symposium school in holography, coherent optics and photonics: Proceedings of symposium school. Ed. by Cand. Sci. I.V. Alekseienko]. Kaliningrad: BFU; 2017. pp. 122-123

[43] Vladimirov AP, Korovin BB, Chervoniuk VV. K razrabotke sredstv kontrolia vibratsiy rabochih lopatok GTD s ispolzovaniiem metoda dinamicheskogo speckl-interferometricheskogo opredeleniia deformatsii. Perspectivy razvitiia aviatsionnyh kompleksov gosudarstvennoi aviatsii i ih silovyh ustanovok. Sbornik nauchnyh statei po materialam V Mezhdunarodnoi nauchno-practicheskoi konferentsii "Zhukovskiie akademicheskiie chteniia" [On developing facilities for monitoring the vibrations of GTE blades using speckle interferometry for strain determination/Development prospects of state aircraft systems and their power units. Collected papers based on Proceedings of V International Applied Science Conference "Zhukovsky Academic readings"]; 22–23 Nov. 2017. Voronezh; 2018. pp. 79-84

[44] Vladimirov AP. Chetyrehmernaiia spekl-tomografiia zhivyh I tehnicheskih tonkih ob'iektov: Teoreticheskaia baza, eksperimenty, dostizheniia i problemy. XXX Mezhdunarodnaia shkola-simposium po golographii, kogerentnoi optike I fotonike: Materialy shkoly-simposiuma . Pod red. kand. fiz.-mat. nauk I.V. Alekseienko [Four-dimensional speckle tomography of live and technical thin objects: Theoretical underpinning, experiments, advances and problems. In: XXX International symposium school in holography, coherent optics and photonics: Proceedings of symposium school. Ed.

by Cand. Sci. I.V. Alekseienko].
Kaliningrad: BFU; 2017. pp. 48-49

[45] Vladimirov AP. Four-dimensional
speckle-interferometric microscopy of
thin biological objects. In: Book of
Abstracts of 5th International Congress
on Microscopy & Spectroscopy
(INTERM 2018). Oludeniz, Turkey.
April 24–30. 2018; p. 36